^{57}Fe and ^{1}H Electron–Nuclear Double Resonance of Three Doubly Reduced States of *Escherichia coli* Sulfite Reductase†

John F. Cline,‡ Peter A. Janick,§ Lewis M. Siegel,*,§ and Brian M. Hoffman*,‡

Department of Chemistry, Northwestern University, Evanston, Illinois 60201, and Department of Biochemistry, Duke University Medical Center and Veterans Administration Hospital, Durham, North Carolina 27705

Received November 13, 1985; Revised Manuscript Received March 14, 1986

ABSTRACT: We have employed electron–nuclear double resonance (ENDOR) spectroscopy to study the ^{57}Fe hyperfine interactions in the bridged-siroheme [4Fe–4S] cluster that forms the catalytically active center of the two-electron-reduced hemoprotein subunit of *Escherichia coli* NADPH–sulfite reductase (SiR^{2-}). Previous electron paramagnetic resonance (EPR) and Mössbauer studies have shown that this enzyme oxidation state can exist in three distinct spectroscopic forms: (1) a "$g = 2.29$" EPR species that predominates in unligated SiR^{2-}, in which the siroheme Fe^{2+} is believed to be in an $S = 1$ state; (2) a "$g = 4.88$" type of EPR species that predominates in SiR^{2-} in the presence of small amounts of guanidinium sulfate, in which the siroheme Fe^{2+} is in an $S = 2$ state; and (3) a classical "$g = 1.94$" type of EPR species that is seen in SiR^{2-} ligated with CO, in which the siroheme Fe^{2+} is in an $S = 0$ state. In all three species, the cluster is in the $[4Fe–4S]^{1+}$ state, and two distinct types of Fe site are seen in Mössbauer spectroscopy. ENDOR studies confirm the Mössbauer assignments for the cluster ^{57}Fe in the $g = 1.94$ state, with A values of 37, 37, and 32 MHz for site I and ca. 19 MHz for site II. The hyperfine interactions are not too different on the $g = 2.29$ state, with site I Fe showing more anisotropic A values of 32, 24, and 20 MHz (site II was not detected). The ^{57}Fe ENDOR spectra of the $g = 4.88$ species are markedly different, however, with ^{57}Fe hyperfine interactions from three, and most probably four, distinct sites being detected; all but one exhibit unusually anisotropic couplings. This degree of resolution of iron sites in a $[4Fe–4S]^{1+}$ cluster is unprecedented. We have examined the ^{57}Fe hyperfine interactions with the spin-coupling models previously developed to describe the g values of the SiR^{2-} forms. The unusual properties of the iron sites within the cluster of the $g = 4.88$ form of SiR^{2-} are not readily interpreted as simple manifestations of weak spin coupling between $S = 2$ ferroheme and unperturbed cluster and may well reflect real physical and/or chemical differences between the cluster in the $g = 4.88$ state and in the well-characterized $g = 1.94$ state.

The hemoprotein subunit of *Escherichia coli* sulfite reductase contains a novel catalytically active center comprised of a siroheme linked to a [4Fe–4S] cluster (Siegel et al., 1982; Christner et al., 1981). The oxidized enzyme as isolated has been studied by optical, EPR,[1] Mössbauer, and ENDOR[1] spectroscopies (Janick & Siegel, 1982; Siegel et al., 1982; Christner et al., 1981; Cline et al., 1985). These studies show that in this enzyme form (SiR^{o}) the heme is in the high-spin, Fe(III) state and the cluster is in the $[4Fe–4S]^{2+}$ (oxidized ferredoxin) state that has exchange coupling between the heme and one Fe atom of the cluster that presumably arises from a covalently linked bridging ligand. ENDOR studies on SiR^{o} rule out imidazolate as a bridge (Cline et al., 1986) and are consistent with preliminary fits of a cysteinyl residue to the electron density between heme and cluster.[2]

Janick and Siegel (1982, 1983) have shown that native SiR^{o} can be reduced by two electrons; the first reduces the heme iron from the high-spin ferric state to a ferrous form, which is EPR silent, whereas the second is accommodated by the iron–sulfur cluster. The two-electron-reduced native enzyme, SiR^{2-}, exhibits three distinctive types of EPR signal: a novel signal with g values at 2.53, 2.29, and 2.07 (referred to as "$g = 2.29$" state) (0.63 spin per heme); spectra from two "$S = {}^{3}/_{2}$ type" species, together accounting for 0.16 spin per heme; and a very small amount of the classical "$g = 1.94$" type of EPR signal from a $[4Fe–4S]^{1+}$ center (0.03 spin per heme). CO binds to the ferroheme of SiR^{2-} to give SiR^{2-}–CO. In this state, only the $g = 1.94$ signal, typical for a magnetically isolated $[4Fe–4S]^{1+}$ cluster system, is observed (ca. 1.0 spin per heme). Addition of small amounts (0.1 M) of the chaotrope guanidinium sulfate to SiR causes the spectrum of fully reduced enzyme to show primarily the $S = {}^{3}/_{2}$ type species with $g = 4.88$, 3.31, and 2.08 (0.7 spin per heme) (referred to as the "$g = 4.88$" state). A similar type of EPR spectrum is seen in SiR^{2-} to which potential weak field heme ligands, such as chloride, have been added.

Despite the differences in the EPR spectra of the three forms of SiR^{2-}, Mössbauer results (Christner et al., 1983a,b, 1984) show that each type of EPR signal is associated with an $S = {}^{1}/_{2}$ $[4Fe–4S]^{1+}$ cluster whose properties appear to be roughly

† The work at Northwestern University was supported by Grant HL-13531 from the National Institutes of Health. The work at Duke University Medical Center and Veterans Administration Hospital was supported by Grant GM-32210 from the National Institutes of Health and Project Grant 7875-01 from the Veterans Administration.

‡ Northwestern University.

§ Duke University Medical Center and Veterans Administration Hospital.

[1] Abbreviations: ENDOR, electron–nuclear double resonance; EPR, electron paramagnetic resonance; Fe_4S_4, tetrairon iron–sulfur center; SiR, sulfite reductase hemoprotein subunit; SiR^{o}, oxidized SiR; SiR^{2-}, two-electron reduced form of SiR; SiR^{2-}–$(Gdm)_2SO_4$, SiR^{2-} in the presence of guanidinium sulfate; SiR^{2-}–CO ("$g = 1.94$ species"), CO-bound SiR^{2-}; "$g = 2.29$ species", SiR^{2-} form exhibiting a characteristic $g = 2.29$ EPR signal; "$g = 4.88$ species", SiR^{2-} form exhibiting a characteristic $g = 4.88$ EPR signal; EDTA, ethylenediaminetetraacetic acid.

[2] X-ray studies by D. E. McRee, D. C. Richardson, J. C. Richardson, and L. M. Siegel, unpublished results; ENDOR comparison by L. Siegel and B. M. Hoffman, unpublished results.

0006-2960/86/0425-4647$01.50/0

the same in all three states. The Mössbauer analysis of Christner et al. (1984) suggests that the EPR spectra are different because the cluster is spin-coupled to the ferroheme, which adopts different spin states in the different forms and alters the magnetic properties of the coupled heme–cluster center. In SiR^{2-}–CO the siroheme iron is inferred to be low-spin ferrous ($S_h = 0$), and the EPR signal is typical of a $[4Fe–4S]^{1+}$ cluster unperturbed by a paramagnetic heme ion. The unusual g values of the SiR^{2-} $g = 2.29$ species are attributed to spin coupling between this cluster and a siroheme ferrous iron that is probably in the $S_h = 1$ state. The similarity of the $g = 4.88$ species EPR signal to that of a true $S = {}^3/_2$ center is only fortuitous, and the signal instead arises through weak exchange coupling of the cluster ($S_c = {}^1/_2$) with a high-spin ferrous heme ($S_h = 2$).

Mössbauer results from the $[4Fe–4S]^{1+}$ cluster of SiR^{2-}–CO have been analyzed in detail. They indicate that the four sites of the iron–sulfur cluster are equivalent in pairs, termed sites I and II, as is true for the resting state SiR° (Christner et al., 1981, 1983). In SiR^{2-}–CO, the magnetic hyperfine interaction of site I is isotropic whereas site II is characterized by an A tensor with substantial anisotropy (also see Table I). By comparison of the parameters with other $[4Fe–4S]^{1+}$ cluster systems, site I has features more reminiscent of ferric ions whereas site II has increased ferrous character. Since the g values of SiR^{2-}–CO are virtually isotropic, it was not possible to correlate the components of the g and A tensors.

Such a detailed analysis of the properties of the $[4Fe–4S]^{1+}$ cluster by Mössbauer spectroscopy (Christner et al., 1983a,b, 1984) was not possible for the $g = 2.29$ and $g = 4.88$ forms because SiR^{2-} samples containing only these species free of any of the other EPR forms could not be prepared. It was concluded that the general features of the $[4Fe–4S]^{1+}$ cluster of SiR^{2-}–CO are unaltered in the $g = 2.29$ and $g = 4.88$ species, but this conclusion was based on a qualitative comparison between the spectrum of the $[4Fe–4S]^{1+}$ cluster of SiR^{2-}–CO with Mössbauer spectra of enzyme samples in which one or the other of the $g = 2.29$ or 4.88 species was in the majority. The limitations of the Mössbauer analysis for SiR^{2-} have been discussed by Christner et al. (1984).

To characterize the iron sites in the $[4Fe–4S]^{1+}$ cluster of SiR^{2-} more fully, particularly for the less well characterized $g = 2.29$ and $g = 4.88$ species, we have extended our ENDOR measurements to examine the three forms of SiR^{2-}. ENDOR is in effect a nuclear magnetic resonance technique in which one obtains electron–nuclear hyperfine couplings of a paramagnetic center by inducing nuclear resonance transitions while monitoring changes in the center's EPR signal. With ENDOR one is able to look separately at individual species in a mixture by selecting appropriate field positions, and thus the technique is particularly well suited for the study of systems, such as SiR^{2-}, exhibiting a suite of forms that cannot be prepared in a pure state. The results of this ENDOR analysis of SiR^{2-} form the subject of this paper.

Materials and Methods

E. coli NADPH–sulfite reductase (a complex of the catalytically active hemoprotein subunit with a specific flavoprotein), natural abundance Fe (termed ^{56}Fe enzyme), was purified by the procedure of Siegel et al. (1973). To obtain ^{57}Fe-enriched enzyme, *E. coli* K12 cells were grown as previously described (Siegel et al., 1973) with 0.5 mg per ^{57}Fe (95% enrichment, New England Nuclear), and the NADPH–sulfite reductase was purified by the same procedure. With both enzyme samples, the SiR° hemoprotein subunit was isolated as described by Siegel and Davis (1974). The enzyme was buffered in 0.1 M potassium phosphate, pH 7.7, containing 0.1 M EDTA, and stored frozen in liquid N_2 prior to use. Siroheme concentration of SiR° samples were determined optically by using $\epsilon_{591} = 1.8 \times 10^4$ M^{-1} cm^{-1} (Siegel et al., 1982).

Reduction of SiR samples to the two-electron-reduced state was achieved with the photoreduction procedure of Massey and Hemmerich (1978) as described in detail by Janick and Siegel (1982). In all cases, ENDOR tubes contained anaerobic solutions of 200–300 μM SiR, 0.1 M potassium phosphate (pH 7.7), 10 mM EDTA, and a deazaflavin/SiR ratio of 0.20. For preparation of "native" SiR^{2-}, there were no additions to the solution. For preparation of SiR^{2-}–CO, the solution was saturated with CO. For preparation of SiR^{2-}–$(Gdm)_2SO_4$, the solution contained 0.1 M guanidinium sulfate. Samples were placed in a chromatography tank filled with ice water (to prevent overheating) and subjected to periods of illumination with a General Electric 200-W "narrow spot" sealed beam lamp. At intervals, the samples were removed from the bath and optical spectra recorded with an Aminco DW-2 dual-beam spectrophotometer equipped with a special holder to permit measurements on EPR/ENDOR tubes and an Aminco microcondenser accessory [refer to Janick and Siegel (1982)] in order to follow the degree of enzyme reduction. When the optical spectra showed that photoreduction was complete, the samples were frozen in liquid nitrogen for storage prior to EPR and ENDOR analysis.

The ENDOR spectrometer is based on a modified Varian E109 EPR spectrometer. Experiments were performed with a silvered brass TE_{102} cavity (Venters et al., 1986) held at 2.0 K in a Janis Corp. immersion Dewar. Normally, spectra were taken at ca. 9.5 GHz; selected spectra employed 10 and 8.7 GHz. The radio frequency (rf) was provided by a Hewlett-Packard (HP) Model 8601A rf generator driven by a linear voltage ramp from a Nicolet Model 1280 computer. The rf power was amplified by Electronic Navigation Instruments (ENI) Model A150 or 3200L 150-W amplifier. A radio-frequency power of 20 W gave $\sim$1 G in the rotating frame. The ENDOR signals were observed as a decrease in the 100-kHz modulated, dispersion-mode EPR signal and accumulated in the computer. All ENDOR patterns were observed with both increasing and decreasing frequency sweeps; parameters reported are the average of these measurements.

ENDOR is performed at a fixed applied field H_0 and is manifested by changes in the EPR signal intensity that result from nuclear transitions induced by a swept radio-frequency field (Abragam & Bleaney, 1970; Atherton, 1973). A set of magnetically equivalent protons is expected to give a single pair of ENDOR transitions separated by the angle-dependent hyperfine coupling constant A^h and mirrored about the free-proton Larmor frequency $\nu_H = g_H\beta_n H_0/h$ (14.69 MHz at 3450 G) according to the equation (Atherton, 1973)

$$\nu_\pm^H = \nu_H \pm A^H/2 \quad (1)$$

The ENDOR pattern of an individual ^{57}Fe nucleus, or a set of magnetically equivalent nuclei, consists of a pair of lines centered at half the hyperfine coupling $A/2$ and split by twice the nuclear Larmor frequency ν_{Fe}:

$$\nu_\pm^{Fe} = A^F/2 \pm \nu^{Fe} \quad (2)$$

For an $S = {}^1/_2$ spin system without low-lying excited states, $\nu_{Fe} = \nu_{Fe}^0 = g_{Fe}\beta_n H_0$, which is small ($\nu_{Fe}^0 = 0.14$ MHz at 1000 G, 0.47 MHz at 3450 G), and the splitting often is not resolved. For a system with $S > {}^1/_2$, such as a high-spin ($S = 2$) ferroheme, the pseudonuclear Zeeman effect can greatly modify ν_{Fe} (see the Appendix).

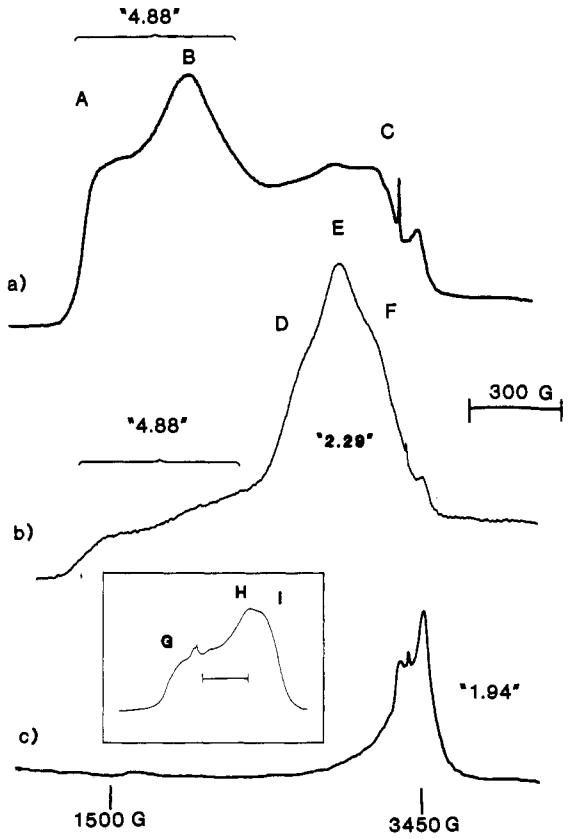

FIGURE 1: Dispersion-mode EPR spectra of three two-electron-reduced forms of sulfite reductase recorded at 2 K, 9.6-GHz microwave frequency, 0.2-mW microwave power, and 5-G modulation amplitude. Positions A–I indicate positions of ENDOR spectra. (a) SiR^{2-}–$(Gdm)_2SO_4$, g = 4.88 species is in the majority, but g = 2.29 and g = 1.94 species are also present. (b) Unligated SiR^{2-}: g = 2.29 species is in the majority with some g = 4.88 and g = 1.94 species impurities. (c) SiR^{2-}–CO: only a typical g = 1.94 type $[Fe_4S_4]^{1+}$ cluster signal is observed. Inset: expanded view of SiR^{2-}–CO, indicating position of ENDOR spectra. Scale indicator represents 100 G.

The ^{57}Fe ENDOR patterns obtained from frozen solutions are analyzed through use of the simulation procedure described earlier (Hoffman et al., 1984, 1985). The hyperfine parameters reported below (Table I) are derived in terms of an effective-spin $S' = {}^1/_2$ Hamiltonian describing the lowest Kramers doublet for the heme–cluster system as a whole:

$$\hat{H} = \hat{S}'gH + \hat{S}\sum A^i\hat{I}_i \qquad (3)$$

However, the g tensor and A tensors for the g = 2.29 and g = 4.88 states are the result of spin coupling between cluster and heme spins. The Appendix summarizes and extends the coupling scheme proposed by Christner et al. (1984) with emphasis on the application to the analysis of hyperfine interactions with ^{57}Fe sites of the g = 4.88 species.

Results and Theory

EPR Spectra. Figure 1 presents the field-modulated, dispersion-mode EPR spectra of the three forms of SiR^{2-}; these signals were obtained under conditions of rapid adiabatic passage induced by the 100-kHz field modulation and correspond to the respective EPR absorption-mode envelopes not the dispersion derivatives. The g = 1.94 signal of Figure 1c and inset is characteristic of a $[4Fe–4S]^{1+}$ cluster; observed g values are given in Table I. The spectrum is indicative that only a single type of reduced enzyme species is present, and when the field is set at the extreme edges of the spectrum (positions G and I in inset of Figure 1c), one obtains single-crystal-like ENDOR patterns, associated with those molecules of SiR^{2-}–CO having the magnetic field directed along the g-tensor axes associated with the largest and smallest g values (Venters et al., 1986).

The EPR spectrum of SiR^{2-}–CO, shown in Figure 1c, is compared to spectra of samples of SiR^{2-} in the unligated state (Figure 1b) and in the presence of $(Gdm)_2SO_4$ (Figure 1a). It is clear from the EPR spectrum of unligated SiR^{2-} (Figure 1b) that more than one species is present, as would be expected from the results of Janick and Siegel (1982). The major component, referred to as the g = 2.29 species, has g values of 2.53, 2.29, and 2.07, corresponding to positions D, E, and F of Figure 2b. The minor components of the so-called 4.88 type (g values of 4.88, 3.31, and 2.08, seen in the bracket region) and 1.94 type also show appreciable intensity in the EPR spectrum. Although the overlap from the EPR signals of multiple species can interfere with ENDOR measurements, in this sample, intensity from the 2.29 species is considerably stronger than the intensity due to any of the other species within the field range of its absorption envelope, and this enzyme form thus dominates the ENDOR spectrum of the unligated SiR^{2-}.[2]

The EPR spectrum of SiR^{2-}–$(Gdm)_2SO_4$ (Figure 1a) contains a majority of what is called the g = 4.88 form having g values of g = 4.88, 3.31, and 2.08 (~70%); the g = 2.29 and 1.94 forms contribute ~30% to the EPR signal. However, the two minority species do not contribute to the EPR intensity at fields lower than that marked B, and thus only the g = 4.88 form will give ENDOR spectra associated with those magnetic field positions.

^{57}Fe ENDOR of SiR^{2-}–CO (g = 1.94 Species). ENDOR spectra taken at a microwave frequency of 9.53 GHz (not shown) show ^{1}H resonances with a high-frequency shoulder. To better resolve this shoulder, ENDOR experiments were performed at 8.7 GHz; this shifts the center of the ^{1}H pattern to a lower frequency but leaves any ^{57}Fe resonance relatively unchanged. All of the ENDOR results reported for the SiR^{2-}–CO were taken at 8.7 GHz.

The broad-band, g = 1.91 ENDOR spectra (position I of Figure 1c, inset) obtained from ^{57}Fe-enriched and natural abundance SiR^{2-}–CO are presented in parts a and c and parts b and c, respectively, of Figure 2. The feature labeled a,a′ in Figure 2b is centered at the free-proton Larmor frequency (ν_H) and represents proton ENDOR. These resolve into multiple-resolved Larmor doublets under other conditions. In the ^{57}Fe-enriched protein (Figure 2a), a ^{57}Fe ENDOR feature that exhibits a splitting of $2\nu_{Fe}$ (eq 2) and is not present with the natural abundance sample (Figure 2b) is clearly visible on the high-frequency side of the proton resonances. At higher microwave power the proton resonances of the natural abundance protein change minimally, becoming somewhat asymmetric and less resolved (Figure 2d), but the ENDOR spectrum of the ^{57}Fe-enriched protein changes dramatically (Figure 2c). In Figure 2c proton peak a′ has been suppressed; the ^{57}Fe resonance is more intense and of opposite phase to that of the proton resonances. This response to microwave power is a very useful tool in assigning ^{57}Fe resonances in spectra obtained at other field positions. ENDOR spectra that were taken at intermediate field values (e.g., g = 1.93, position H of Figure 1c, inset) also show an iron ENDOR feature around 18.5 MHz that reverses phase with increased microwave power (~0.2 mW); in addition, there is some intensity around 9.5 MHz in the ^{57}Fe-enriched protein that may perhaps be associated with the second iron site of the Fe_4S_4 cluster.

The ENDOR spectra (not shown) obtained with the field set to the low-field edge of the EPR spectrum, corresponding

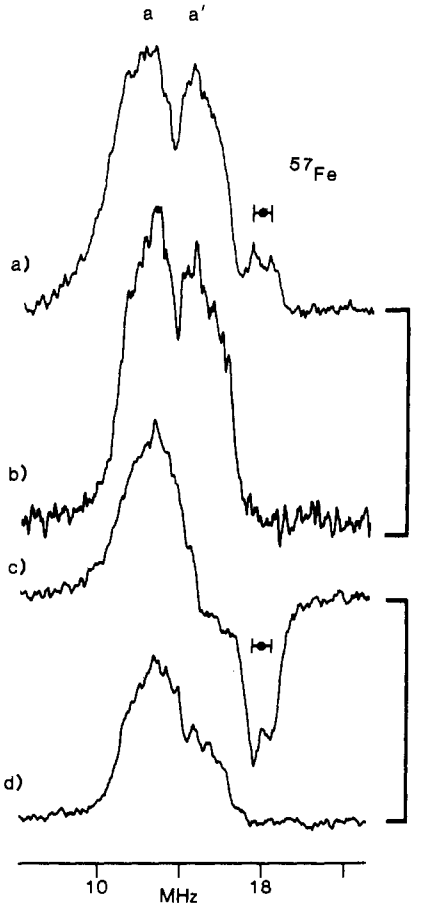

FIGURE 2: Broad-band ENDOR spectra of SiR^{2-}–CO at $g = 1.91$ (H_0 set to position I of Figure 1, inset): ^{57}Fe enriched (a and c); native ^{56}Fe (b and d). Proton resonances are indicated as a and a'; ^{57}Fe resonances are indicated by their center frequency $A^{Fe}/2$ (●) and by $2\nu^{Fe}$ (|–●–|). Conditions: (a and b) microwave frequency, 8.699 GHz; H_0 = 3265 G; T = 2 K; microwave power, 0.6 μW; 100-kHz field modulation, ~5 G; rf power, 20 W; rf scan rate, 3.5 MHz/s; (c and d) microwave power, 0.06 mW; other conditions as in (a and b).

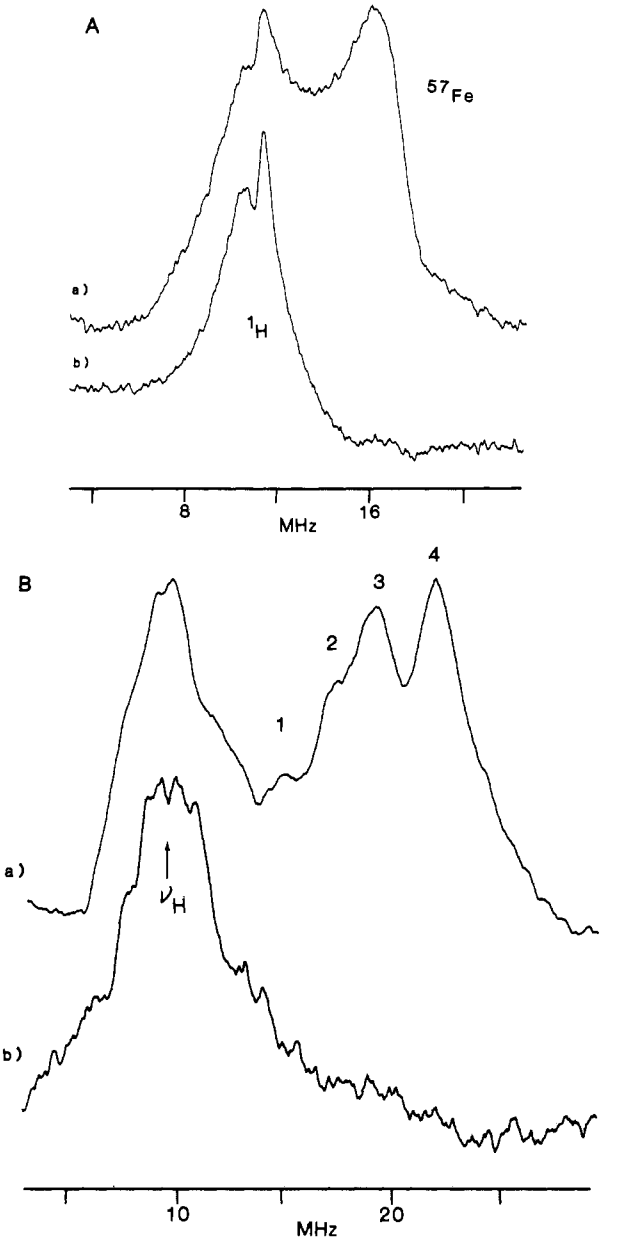

FIGURE 3: Broad-band ENDOR spectra of two-electron-reduced forms of sulfite reductase (note differences in scale between panels A and B). (A) $g = 2.29$ species of unligated SiR^{2-} at $g = 2.53$ (H_0 set to position D of Figure 1b): ^{57}Fe enriched (a); native ^{56}Fe (b). Proton resonances shown are centered at the proton Larmor frequency, ν_H. The ^{57}Fe resonance is clearly visible. Conditions: microwave frequency, 9.525 GHz; H_0 = 2650 G; T = 2 K; microwave power, 0.2 mW; 100-kHz field modulation, ~5 G; rf power, 20 W; rf scan rate, 3.5 MHz/s. (B) Broad-band ENDOR of SiR^{2-}–$(Gdm)_2SO_4$, g = 4.88 species, at $g = 4.86$ (H_0 set to position A of Figure 1a): ^{57}Fe enriched (a); native ^{56}Fe (b). Unresolved proton resonances are centered at the proton Larmor frequency, ν_H (eq 1). The ^{57}Fe resonances are designated as peaks 1–4. Conditions: microwave frequency, 9.525 GHz; T = 2 K; microwave power, 0.2 mW; 100-kHz field modulation, ~5 G; rf power, 20 W; rf scan rate, 7.5 MHz/s; H_0 = 1400 G.

to the $g = 2.03$ axis (position G of Figure 1c, inset), are not as straightforward to interpret. Computer subtraction (^{57}Fe – ^{56}Fe) shows features at 9 and 16 MHz that tentatively may be assigned to the ^{57}Fe resonance. The high-frequency feature is confirmed to be a ^{57}Fe resonance by a spectrum at high microwave power that shows the ^{57}Fe resonance with opposite phase compared to the protons. Because of a base-line artifact that occurs in the range 5–10 MHz at high microwave power, we are unable to unambiguously assign a low frequency feature to ^{57}Fe in the high microwave power results.

The hyperfine coupling constants obtained for SiR^{2-}–CO by ENDOR and Mössbauer spectroscopies are presented in Table I. Mössbauer measurements have assigned the four ^{57}Fe sites of the [4Fe–4S] cluster as being of two types, designated site I and site II. The ENDOR spectra contain resonance from one of these two pairs, and the observed hyperfine values correlate well with that designated as site I. The ENDOR results show that the site I couplings are slightly larger and more anisotropic than first thought on the basis of Mössbauer spectroscopy. Moreover, assignment of the observed A values to the principal g values is now possible. The observation of a resonance from the type II sites in ENDOR is tentative, but is consistent with Mössbauer results.

^{57}Fe ENDOR of SiR^{2-} ($g = 2.29$ Species). The low-field, $g = 2.53$, ENDOR spectra (position D, Figure 1b) obtained with ^{57}Fe-enriched and natural abundance unligated SiR^{2-} are presented in parts a and b, respectively, of Figure 3A. The resonance in Figure 3Ab is centered at the free-proton Larmor frequency (ν_H) and represents proton ENDOR. For the ^{57}Fe-enriched protein, an ^{57}Fe ENDOR signal associated with one type of iron site is clearly visible (Figure 3Aa) at higher frequency than the proton resonances. A weak shoulder on the high-frequency side of this ^{57}Fe resonance is due to the ^{57}Fe signal from the weak, underlying EPR spectrum of the $g = 4.88$ species (vide infra). A signal from the second type of iron site suggested by Mössbauer spectroscopy to exist in

Table I: ^{57}Fe Hyperfine Tensor Values (MHz) of SiR^{2-} Forms[a]

		A_α^{Fe} at g_α =		
	site	2.04	1.93	1.91
SiR^{1-}–CO,[b] g = 1.94	I	[−33.7]	[−33.7]	[−31.6]
		37(1)	37(1)	32(1)
	II	[11]	[22.0]	[19.3]
			~19[c]	~19[c]
		A_α^{Fe} at g_α =		
	site	2.53 (y)	2.29 (x)	2.07 (z)
SiR^{2-}, g = 2.29	I	32	24(1)	20(2)
		A_α^{Fe} at g_α =		
	site	4.88 (y)	3.31 (x)	2.08 (z)
SiR^{2-}–$(Gdm)_2SO_4$, g = 4.88	1	41(1)	15(5)	≤10
	2	35(1)	10(5)	≤10
	3	31(1)	10(5)	≤10
	4	27(1)	27(3)	20–30

[a] The hyperfine tensor components have been obtained by analyzing the ENDOR spectra through use of simultations employing the theory of polycrystalline ENDOR spectra (Hoffman et al., 1984). It was adequate to assume coaxial A and g tensors with the correspondence of axes as indicated. Distinguishable sites are labeled I, II, or 1–4. [b] Mössbauer spectroscopic determination (Christner, et al., 1983) provides the values in brackets but does not provide a correspondence between axes; the values are arranged to maximize agreement between techniques. [c] Tentative assignment; see text.

the $[4Fe–4S]^{1+}$ cluster of the g = 2.29 species is not seen in its ENDOR spectrum; the frequency proposed for this site would place the resonance near the proton resonances, thereby making it difficult to see. In ENDOR spectra of the g = 2.29 species taken at a low microwave frequency (8.7 GHz) the protons have moved to a lower frequency (see eq 1), exposing the ^{57}Fe resonance for better observation at intermediate field positions (Figure 4). As the field is increased from g = 2.53 (between positions D and E of Figure 1b), the ^{57}Fe resonance shifts to lower frequency, as a result of anisotropy in the magnetic hyperfine coupling tensor of this iron site. These ENDOR results can be analyzed through the use of the theory of polycrystalline ENDOR (Hoffman et al., 1984), on the basis of coaxial A and g tensors. The tensor values are presented in Table I, and calculated positions of the ^{57}Fe resonances are indicated by arrows in Figure 4. Comparison with previous results indicates that the hyperfine coupling along the g = 2.53 tensor axis is very similar to the average site I ^{57}Fe coupling inferred from Mössbauer results and also shows a hyperfine anisotropy not detected by Mössbauer spectroscopy.

^{57}Fe ENDOR of SiR^{2-} with $(Gdm)_2SO_4$ (g = 4.88 Form). The broad-band, low-field ENDOR spectrum (g = 4.88; position A of Figure 1a) obtained from ^{57}Fe-enriched and natural abundance protein is presented in parts a and b of Figure 3B, respectively. The proton pattern, centered at the proton Larmor frequency (ν_H), is shown in Figure 3Bb. In the ^{57}Fe-enriched protein, four distinct ^{57}Fe ENDOR features are visible and assigned as peaks 1–4. These peaks are much better resolved in the more tightly focused spectra of Figure 5. As is most clearly seen in Figure 3, the exchange coupling between the S = 2 heme and $S = {}^1/_2$ cluster in this species leads to more complex magnetic properties than seen in the g = 2.29 species, or in SiR^{2-}–CO. The frequencies of the ^{57}Fe resonances were monitored as a function of field position (g value) (Figure 5); at higher fields, resolution is lost. The frequency of peak 1 is relatively invariant to changes in the applied field, which indicates that the hyperfine coupling is essentially isotropic. In contrast, peaks 2–4 shift to lower frequency with increasing field, indicating that the hyperfine coupling associated with these resonances is strongly anisotropic.

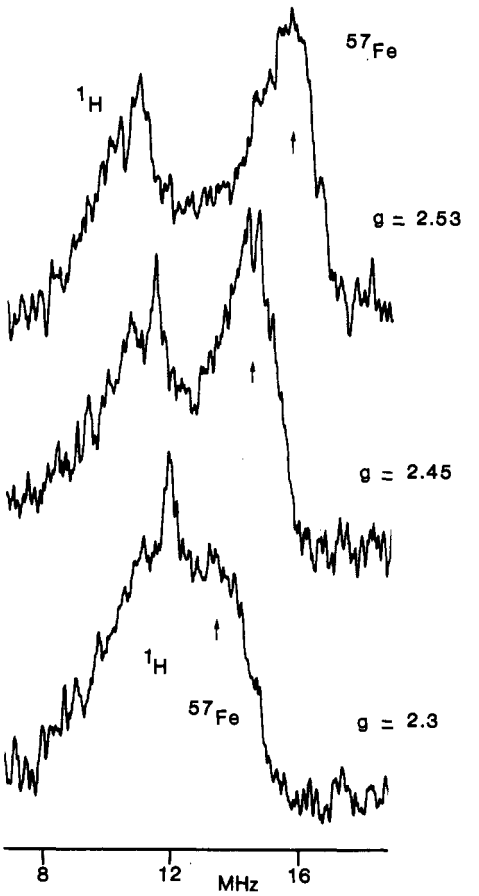

FIGURE 4: ^{57}Fe ENDOR of the g = 2.29 species of unligated SiR^{2-} taken at three different g values. Proton resonances shift to higher frequency with field positions according to eq 1. The ^{57}Fe resonance is seen to shift with g value, indicative of some anisotropy in the ^{57}Fe coupling. Arrows indicate positions of ^{57}Fe resonances calculated by using hyperfine couplings in Table I. Conditions: microwave frequency, 8.7 GHz; T = 2 K; microwave power, 0.2 mW; 100-kHz field modulation, ~5 G; rf power, 20 W; rf scan rate, 3.5 MHz/s.

The four resonances might represent the four different irons of the cluster, with the heme–iron being undetected. However, if the heme–iron is being observed, then it is likely that the small zero-field splittings of the S = 2 ferroheme (Champion et al., 1975a,b) would give rise to a large pseudonuclear Zeeman effect (Appendix), which means that the heme could exhibit a pair of ENDOR peaks whose splitting is proportional to the applied field but is much larger than $2\nu_{Fe}$. To test this, experiments were performed at g = 4.86, with H_0 = 1466 G (9.975 GHz) and H_0 = 1279 G (8.701 GHz). Of the six possible pairings of four peaks, all but one was unamiguously shown to have a separation invariant with field; the separation of peaks 2 and 3 also did not change within experimental error, although these peaks are sufficiently close that the measurement requires confirmation at other fields. On balance, the experiment gives strong support to an assignment of the four ^{57}Fe ENDOR peaks to four distinct iron sites.

Through the use of the theory of polycrystalline ENDOR (Hoffman et al., 1984), we have derived hyperfine tensors for each of the four sites. The strong anisotropy of sites 2–4 was difficult to reproduce and required that the g and hyperfine tensors be approximately coaxial; the resulting principal hyperfine components are listed in Table I. Note that the A_x have a large uncertainty because of the limited range of fields giving resolved spectra; the A_z are not well-defined because the presence of the g = 2.29 and g = 1.94 states in the sample precluded collection of ENDOR spectra corresponding to pure

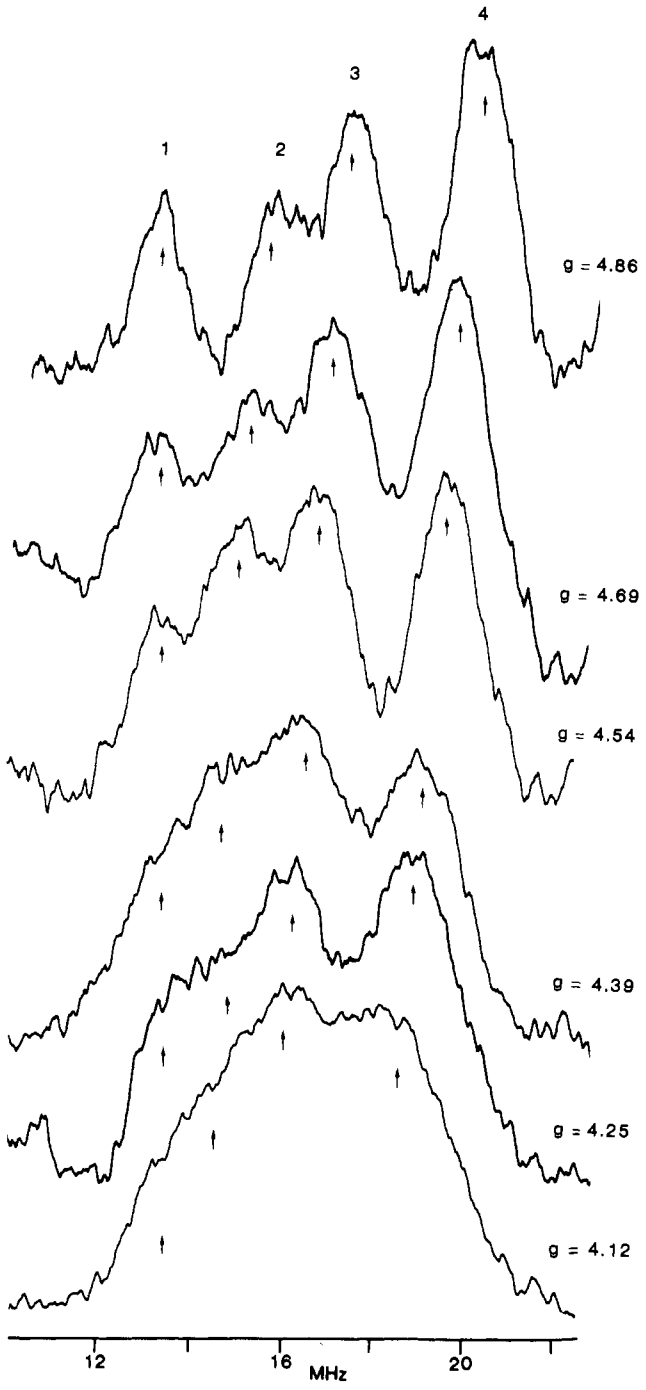

FIGURE 5: ^{57}Fe ENDOR of SiR^{2-}–$(Gdm)_2SO_4$ $g = 4.88$ species; the four ^{57}Fe resonances are labeled as in Figure 3B. As the g value is changed, peak 1 remains at the same frequency, indicating an isotropic hyperfine coupling; peaks 2–4 shift in frequency due to anisotropy in the coupling. Arrows indicate positions of ^{57}Fe resonances calculated by using hyperfine couplings in Table I. Conditions: microwave frequency, 9.525 GHz; $T = 2$ K; microwave power, 0.2 mW; 100-kHz field modulation, ~5 G; rf power, 20 W; rf scan rate, 7.5 MHz/s.

$g = 4.88$ at field values approaching $g = 2.08$. Nevertheless, the calculated positions of the ^{57}Fe resonances, which are indicated by arrows in Figure 5, are seen to be in reasonable agreement with experiment.

Comparison of the ^{57}Fe ENDOR spectra of the three forms of SiR^{2-} clearly indicate that the iron sites of the SiR^{2-} $g = 4.88$ species have significantly different magnetic properties than those of SiR^{2-} in the $g = 2.29$ or the $g = 1.94$ forms. Whereas the iron sites of the cluster in the $g = 2.29$ and $g = 1.94$ species appear to fall into two pairs, the ENDOR spectra of the $g = 4.88$ from clearly show four distinguishable ^{57}Fe sites. The hyperfine tensors of sites 2–4 are strongly anisotropic; that of site 1 appears roughly isotropic.

Is one of the four ^{57}Fe resonances associated with the heme? The intrinsic hyperfine parameters for an $S = 2$ ferroheme ($\bar{A}^h$; see the Appendix) vary with the heme coordination environment. If, for example, the ferroheme of horseradish peroxidase is an appropriate model (Champion et al., 1975b), then the $\bar{A}^h$ values are small and use of eq 9 (see the Appendix) leads to the conclusion that each of resonances 1–4 arises from a discrete cluster–iron site. If we take the cytochrome P_{450} ferroheme as a model, with hyperfine tensor principal values (−24.7, −17.1, −20.6) MHz (Champion et al., 1975a), then by appropriate assignment of tensor axes it would be possible to use eq 9 to assign either of sites 2 or 3 to the heme–iron. However, the zero-field splitting for a ferroheme (Champion et al., 1975a) might yield a large pseudonuclear Zeeman effect (Appendix) with peaks 2 and 3 representing a doublet whose splitting is proportional to the field, and this does not appear to be the case. Thus, subject to confirmation by measurements at other microwave frequencies, we adopt the view that each resonance is from a distinct *cluster* site. Interestingly, either alternative would leave site 4, whose hyperfine values differ most from those of the unperturbed cluster of SiR^{2-}–CO, as being part of the cluster. This could well mean that iron site 4 is bonded to the group that links heme and cluster.

The four ^{57}Fe resonances for the $g = 4.88$ species represent at least two sites that have hyperfine values substantially different from those of SiR^{2-}–CO. According to eq 10, such changes in the cluster–iron hyperfine interactions upon formation of the $g = 4.88$ species cannot be ascribed to the effect of weak spin coupling on an otherwise unmodified $[4Fe–4S]^{1+}$ cluster. It would appear that the ENDOR results signify one of two possibilities or some combination thereof. Either the $[4Fe–4S]^{1+}$ cluster suffers a significant chemical and/or physical perturbation in the $g = 4.88$ state of SiR^{2-}, or else bonding between ferroheme and cluster in this state is sufficiently strong as to induce a mixing of heme and cluster wave functions that provides a direct interaction between the $S_h = 2$ spin of the heme and the nuclear spins of the cluster–iron sites. The former alternative corresponds to a modification of the electronic structure of the cluster that alters the cluster–spin, nuclear–spin couplings, which changes the $\bar{A}^c$ in eq 4; by eq 8, this changes the measured A^c of eq 3.

The second alternative corresponds to the introduction of a new spin-Hamiltonian term that would add to eq 6 a direct hyperfine interaction between the heme spin, S_h, and the ^{57}Fe nuclear spin of the cluster–iron sites, eq 11. The inclusion of direct coupling to the iron site connected to the bridging ligand is a not unreasonable elaboration of the spin-coupling model. It should be noted, however, that inclusion of direct interactions between S_h and multiple iron sites of the cluster does not strictly fall within the conceptual framework underlying such a model, which involves independent spin systems that are coupled by the exchange term, eq 5, but otherwise unmodified.

A direct heme–spin, cluster–iron interaction does modify the effective hyperfine interaction parameters of the latter, as described by eq 12. In order to use these equations to parametrize the cluster hyperfine tensors, it would be necessary to assume that the intrinsic hyperfine interactions with the cluster spin are the same in SiR^{2-} $g = 4.88$ and in SiR^{2-}–CO and to assign the cluster–iron sites 1–4 in the $g = 4.88$ form to either site I or site II of the CO species. A semiquantitative treatment suggests that the site 1 of SiR^{2-} $g = 4.88$ can be assigned to site I iron that has weak interactions with the

heme–spin. Similarly, one can assign site 4 as a strongly perturbed site II iron, provided that the smallest tensor component is matched appropriately. It is not possible to give a satisfactory assignment of both site 1 and site 2; this may be due either to limitations in the model or to the fact that one resonance belongs to the heme.

Overall, the ^{57}Fe ENDOR analysis suggests that the magnetic properties of the $g = 4.88$ species reflect significant perturbations to the normal electronic structure of the [4Fe–4S]$^{1+}$ cluster in addition to the type of spin coupling to high-spin ferroheme discussed by Christner et al. (1984). Also, it is consistent with the intuitive notion that site 4 of the SiR^{2-} $g = 4.88$ species, which differs most strongly from the cluster sites of SiR^{2-}–CO, represents the cluster–iron attached to the bridging ligand.

Conclusions

These ENDOR studies allow certain detailed comparisons of three distinct species produced by two-electron reduction of *E. coli* sulfite reductase: SiR^{2-}–CO; SiR^{2-} $g = 2.29$ species; SiR^{2-}–$(Gdm)_2SO_4$ $g = 4.88$ species. SiR^{2-}–CO shows a ^{57}Fe ENDOR resonance whose hyperfine coupling is within the range given by Mössbauer spectroscopy for site I of the [4Fe–4S]$^{1+}$ cluster (Christner et al., 1983a,b). The couplings (Table I) are slightly larger than those previously inferred and exhibit a noticeable anisotropy. A second cluster–site II, found by Mössbauer to have an anisotropic coupling, is not clearly visualized in ENDOR but may have been seen as a shoulder on the proton resonances that gives couplings consistent with those previously reported.

In the unligated, SiR^{2-} $g = 2.29$ form, only one ^{57}Fe resonance is seen in ENDOR spectra. The coupling along $g = 2.53$ is very similar to that expected from Mössbauer data for cluster–site I. ENDOR shows that the site I coupling in this form is slightly smaller than that seen in SiR^{2-}–CO and in addition has a much greater anisotropy. There is no evidence in ENDOR of the presence of a ^{57}Fe resonance from a second cluster–iron site. Presumably it is obscured by the proton resonances, although it is conceivable that the observed resonance represents all four of the cluster irons.

Thus ENDOR confirms the basic conclusions of Mössbauer spectroscopy that the [4Fe–4S]$^{1+}$ cluster is very similar in the $g = 2.29$ species and SiR^{2-}–CO (Christner et al., 1983). In addition, we also find that the changes in the spin state of the heme (probable $S = 1$ vs. $S = 0$) in these two enzyme forms causes detectable differences in the magnitude and anisotropy of the cluster–iron hyperfine couplings (Table I).

In contrast, the ENDOR measurements reveal that the properties of iron sites in the [4Fe–4S]$^{1+}$ cluster of the SiR^{2-} $g = 4.88$ form differ significantly from those of the sites in the $g = 2.29$ and SiR^{2-}–CO species. One should note that the resolution of the [4Fe–4S]$^{1+}$ cluster spectrum of SiR^{2-} $g = 4.88$ species into four distinct ^{57}Fe hyperfine interactions (or even three, if one of these lines is due to the heme Fe) represents the first occasion in which such a degree of resolution has been observed in any system containing a [4Fe–4S] cluster. We have recently reported the resolution of five ^{57}Fe hyperfine interactions in the ENDOR spectra of the FeMoco cofactor of nitrogenase (Hoffman et al., 1982; Venters et al., 1986), but this is a chemically more complex entity than a [4Fe–4S] cluster.

The differences among the cluster–irons of SiR^{2-}–$(Gdm)_2SO_4$ and the remarkable hyperfine anisotropy reflect perturbations of the cluster linked to the paramagnetic siroheme Fe^{2+}. The ^{57}Fe hyperfine interaction has been discussed within the spin-coupling model developed to describe the g values of the SiR^{2-} forms (Christner et al., 1984). The unusual properties of the iron sites within the cluster of the $g = 4.88$ form are not readily interpreted as simple manifestations of spin exchange between an $S = 2$ ferroheme and a normal $S = {}^1/_2$ cluster. They appear instead to reflect in some part real chemical and/or physical differences between the cluster in the $g = 4.88$ state and in the well-characterized SiR^{2-}–CO $g = 1.94$ state. It might be that the structure and therefore the electronic properties of the cluster are altered by a protein conformational change or that formation of the $g = 4.88$ form is accompanied by loss or replacement of ligands to the cluster; alternatively, bonding between heme and cluster may be more pronounced in the $g = 4.88$ state of SiR^{2-}. Finally, we note that the $g = 4.88$ type of species seen when SiR^{2-} is perturned by low concentrations of the chaotrope $(Gdm)_2SO_4$ also is the major species seen in enzyme reduced in the presence of the potential weak-field ligand Cl$^-$. It is a minor species in "unligated" SiR^{2-} prepared in phosphate buffer but is the majority form seen in fully reduced spinach nitrite reductase, which possesses a siroheme–Fe_4S_4 active center similar to that seen in SiR (Wilkerson et al., 1983).

Acknowledgments

We thank John F. Madden for his assistance in preparing some of the samples used in this work, Drs. Ryszard J. Gurbiel and Joshua Telser for their assistance in obtaining the multifrequency ENDOR spectra described here, and Dr. E. Münck for helpful discussions.

Appendix

Magnetic Interactions in SiR^{2-}. The [4Fe–4S]$^{1+}$ cluster has a spin $S_c = {}^1/_2$ that results from strong antiferromagnetic interactions among its four iron atoms. The interactions of the cluster spin with an external field and with the ^{57}Fe nuclear spins ($i = 1$–4) are described by a Hamiltonia written in terms of the cluster g tensor (g_c) and the intrinsic hyperfine couplings of the iron sites ($\bar{A}_i^c$), with the third term representing the nuclear Zeeman interaction:

$$\hat{H}_c = \hat{S}_c g_c H + \hat{S}_c \sum \bar{A}_i^c I_i + g_{Fe}\beta_n \sum \hat{I}_i H \qquad (4)$$

A ferrosiroheme that is in the high-spin ($S_h = 2$) state has magnetic properties described by the spin Hamiltonian

$$\hat{H}_h = \hat{H}_{ZFS} + \hat{S}_h g_h H + \hat{S}_h \bar{A}^h \hat{I}_h + \beta_n \hat{I}_n g^{Fe} H \qquad (5)$$

The zero-field splitting (ZFS) term is characterized by the parameters, $D \sim 5$–15 M^{-1}, $E \geq 0$; the g values, $g_{h\alpha}$ ($\alpha = x, y, z$) do not differ greatly from 2. Because of the zero-field splitting, the heme ground state is essentially the $m_h = 0$ singlet, and in the absence of coupling to the $S = {}^1/_2$ cluster, neither the Zeeman (second term) nor hyperfine (third term) interactions give first-order contributions to the energy. The presence of low-lying, $m_h = \pm 1$, heme states can create a pseudonuclear Zeeman effect (Abragam & Bleaney, 1970; Venters et al., 1986). The interaction (term 4) is described by an effective nuclear g^{Fe} tensor that is coaxial with the zero-field splitting tensor and has principal components $g_\parallel^{Fe} = g_{Fe}$ and $g_\perp^{Fe} = g_{Fe}[1 + (g\beta/g_{Fe}\beta_n)(A_i/\Delta)]$, $j = x, y$.

It is assumed by Christner et al. (1984) that the siroheme iron and a single iron site of the cluster, designated site 1, are chemically linked by a bridging group. This produces a weak interaction between heme and cluster spins that is described by an exchange-coupling term

$$\hat{H}_{ex} = k_{1h}\hat{S}_1\hat{S}_h \qquad (6)$$

where $\hat{S}_1$ is the local spin of cluster site 1. However, within

the ground doublet of the $[4Fe-4S]^{1+}$ cluster this interaction can be reexpressed in terms of the cluster spin

$$\hat{H}_{ex} = J\hat{S}_c\hat{S}_h \tag{7}$$

where $J = k_{1h}F_1$ and F_1 is an equivalence factor that depends on the electronic structure of the iron–sulfur cluster and whether the cluster–site 1 is of the site I or site II class. The ground state of the coupled system is a Kramers doublet; in the absence of $\hat{H}_{ex}$ its EPR signal would be associated solely with the cluster, and the g and hyperfine values would be those of the cluster. The influence of $\hat{H}_{ex}$ can be understood by treating the exchange with second-order perturbation theory for nondegenerate states in the regime $J/D \ll 1$. $\hat{H}_{ex}$ acts to mix the heme $m_H = \pm 1$ states into the zero-order ground state, thereby modifying its EPR parameters. When quadratic terms are neglected, the g values for the coupled system become

$$g_{x,y} = g_c - 6(J/D)(1 \mp 3E/D)g_{hx,y}$$
$$g_z \approx g_c \tag{8}$$

From the experimental g values for the $g = 4.88$ species (Table I), these equations yield $J/D = -0.15$ and $E/D \sim 0.11$; the exact solution yielded $J/D = -0.22$. Thus, a weak exchange interaction that minimally perturbs the individual heme and cluster components can cause the observed g values to differ markedly from those of the isolated cluster.

If the same treatment is applied to the ^{57}Fe hyperfine couplings, one finds that spin exchange introduces into eq 3 a hyperfine interaction with the heme–iron having tensor components

$$A^h_{x,y} = -6(J/D)(1 \mp 3E/D)\bar{A}^h_{x,y}$$
$$A^h_z \approx 0 \tag{9}$$

where the A^h_α and $\bar{A}^h_\alpha$ represent the hyperfine parameters in eq 3 and 5 respectively. In contrast, the observed hyperfine interactions of the ^{57}Fe nuclei of the cluster are unmodified by exchange with the heme, namely

$$A^c_{i\alpha} \approx \bar{A}^c_{i\alpha} \tag{10}$$

where $A_{i\alpha}$ and $\bar{A}^c_{i\alpha}$ ($\alpha = x, y, z$) represent the coupling constants in eq 3 and 4, respectively. These conclusions are borne out by the exact calculations. Direct coupling of the heme spin to the cluster irons introduces a tensor

$$\hat{H}_{hc} = \sum_{Fe}\hat{S}_h\bar{A}^{hc}_i\hat{I}_i \tag{11}$$

where $\bar{A}^{hc}$ represents this coupling. Upon inclusion of $\hat{H}_{hc}$, the perturbation treatment of cluster–heme exchange does alter the cluster–iron hyperfine interaction tensors that appear in eq 3 and govern the observed ENDOR frequencies

$$A^c_{x,y} = \bar{A}^c_{x,y} - (6J/D)(1 \mp 3E/D)\bar{A}^{hc}_{x,y}$$
$$A_z = \bar{A}^c_z \tag{12}$$

Registry No. ^{57}Fe, 14762-69-7; NADPH sulfite reductase, 9029-35-0; siroheme, 52553-42-1.

References

Abragam, A., & Bleaney, B. (1970) *Electron Paramagnetic Resonance of Transition Ions*, Clarendon Press, Oxford.

Atherton, N. M. (1973) *Electron Spin Resonance*, Wiley, New York.

Champion, P. M., Lipscomb, J. D., Münck, E., Debrunner, P., & Gunsalus, I. C. (1975a) *Biochemistry 14*, 4151–4158.

Champion, P. M., Chiang, R., Münck, E., Debrunner, P., & Hager, L. P. (1975b) *Biochemistry 14*, 4159–4161.

Christner, J. A., Münck, E., Janick, P. A., & Siegel, L. M. (1981) *J. Biol. Chem. 256*, 2098–2101.

Christner, J. A., Münck, E., Janick, P. A., & Siegel, L. M. (1983a) *J. Biol. Chem. 258*, 11147–11156.

Christner, J. A., Janick, P. A., Siegel, L. M., & Münck, E. (1983b) *J. Biol. Chem. 258*, 11157–11164.

Christner, J. A., Münck, E., Kent, T. A., Janick, P. A., Salerno, J. C., & Siegel, L. M. (1984) *J. Am. Chem. Soc. 106*, 6786–6794.

Cline, J. F., Janick, P. A., Siegel, L. M., & Hoffman, B. M. (1985) *Biochemistry 24*, 7942–7947.

Hoffman, B. M., Venters, R. A., Roberts, J. E., Nelson, M. J., & Orme-Johnson, W. H. (1982) *J. Am. Chem. Soc. 104*, 860–862.

Hoffman, B. M., Martinsen, J., & Venters, R. A. (1984) *J. Magn. Reson. 59*, 110–123.

Hoffman, B. M., Venters, R. A., & Martinsen, J. (1985) *J. Magn. Reson. 62*, 537–542.

Janick, P. A., & Siegel, L. M. (1982) *Biochemistry 21*, 3538–3547.

Janick, P. A., & Siegel, L. M. (1983) *Biochemistry 22*, 504–514.

Massey, V., & Hemmerich, P. (1978) *Biochemistry 17*, 9–17.

Siegel, L. M., & Davis, P. S. (1974) *J. Biol. Chem. 249*, 1587–1598.

Siegel, L. M., Murphy, M. J., & Kamen, M. (1973) *J. Biol. Chem. 248*, 251–264.

Siegel, L. M., Rueger, D. C., Barker, M. J., Krueger, R. J., Orme-Johnson, N. R., & Orme-Johnson, W. H. (1982) *J. Biol. Chem. 257*, 6343–6350.

Venters, R. A., Nelson, M. J., McLean, P. A., True, A. E., Levy, M. A., Hoffman, B. M., & Orme-Johnson, W. H. (1986) *J. Am. Chem. Soc. 108*, 3487–3498.

Wilkerson, J. O., Janick, P. A., & Siegel, L. M. (1983) *Biochemistry 22*, 5048–5054.